The Astrophysical Journal, 592:L79–L82, 2003 August 1

INDICATIONS OF INFLOW MOTIONS IN REGIONS FORMING MASSIVE STARS

Jingwen Wu and Neal J. Evans II
Department of Astronomy, University of Texas at Austin, 1 University Station, C1400, Austin, Texas 78712-0259;
jingwen@astro.as.utexas.edu, nje@astro.as.utexas.edu
Received 2003 April 30; accepted 2003 June 23; published 2003 June 26

ABSTRACT

Observational evidence of inflowing motions in massive star-forming regions has been extremely rare. We have made a spectroscopic survey of a sample of 28 massive star-forming cores associated with water masers. An optically thick line of HCN (3–2) was used in combination with optically thin lines [$H^{13}CN$ (3–2) or $C^{34}S$ (5–4), (3–2), and (2–1)] to identify "blue" line profiles that can indicate inflow. Comparing intensities for 18 double-peaked line profiles yields 11 blue and three red profiles that are statistically significant. In the full sample of 28 sources, 12 show blue profiles, and six show red profiles that are statistically significant based on the velocity offsets of lines that are optically thick from those that are optically thin. These results indicate that HCN (3–2) emission may trace inflow in regions forming high-mass stars.

Subject headings: ISM: molecules — stars: formation

1. INTRODUCTION

Gravitational collapse is a widely accepted theoretical explanation of star formation, but the observational evidence of collapse has long been controversial (e.g., Evans 1991; Myers, Evans, & Ohashi 2000). The major difficulty is that collapse proceeds at a relatively low velocity and is easily masked by other motions (e.g., outflows, rotation, and turbulence) in the cloud cores. A general prediction of collapse models is a "blue profile," a line asymmetry with the peak skewed to the blue side in optically thick lines, while an optically thin line must peak at the absorption part (usually a dip) of the optically thick line to rule out the possibility of two velocity components.

For an individual source, one must exclude rotation or outflow blobs as the source of the blue profile by mapping the source. However, the predominance of blue profiles in a survey, based on some objective criteria, can be an indication that inflow is a statistically likely explanation. We use the term "inflow" to distinguish evidence of inflowing motions from a claim of gravitational collapse or infall. A profile that survives these tests provides a strong indication of inflow, and the source can be seen as a collapse candidate. To become a credible example of gravitational collapse, gravity must be a plausible source of the motions, and the line profiles should agree with some detailed model (Evans 2003).

Progress has been made in the last decade in studying low-mass star-forming regions, triggered by the observation of blue profiles toward B335 in lines of H_2CO and CS and later by the fitting (Zhou et al. 1993, 1994; Choi et al. 1995) of these lines with an inside-out collapse model (Shu 1977). Systematic surveys have been made, and predominantly blue profiles have been found toward Class 0 (Gregersen et al. 1997; Mardones et al. 1997), Class I (Gregersen et al. 2000), and Class -1 (also known as pre-protostellar cores) sources (Gregersen & Evans 2000; Lee, Myers, & Tafalla 1999, 2001). Evidence of collapse has been increasingly accepted in low-mass star-forming regions.

Evidence of inflow has been elusive in massive star-forming regions, partly because of the extremely complex and turbulent environment in massive clouds. Spectral inflow signatures have been reported in a few sources, including NGC 2264 IRS (Wolf-Chase & Gregersen 1997), W49 (Welch et al. 1988; Dickel & Auer 1994), G10.6−0.4 (Keto, Ho, & Haschick 1988), and W51 (Zhang & Ho 1997; Zhang, Ho, & Ohashi 1998). However, surveys have not revealed statistical evidence of inflow (e.g., Williams & Myers 1999).

The characteristic blue profile will appear only if the molecular tracer has a suitable optical depth and critical density. For example, using moderately opaque tracers H_2CO and CS, which are good tracers of blue profiles in Class 0 sources, Mardones et al. (1997) found a low fraction of blue profiles in a sample of Class I sources. With a more opaque line of HCO^+ (3–2), Gregersen et al. (2000) detected a blue fraction in Class I sources comparable to that in Class 0 sources. The inflow tracers used in low-mass cores may no longer be suitable for probing inflow motion in high-mass cores, which are typically 100 times denser at a given radius than low-mass cores (Mueller et al. 2002). In a recent survey for blue profiles in high-mass star-forming regions, Williams & Myers (1999) used CS (2–1) (whose critical density n_c is 3.9×10^5 cm^{-3} at $T_K = 100$ K) as the optically thick line. Three out of 19 sources showed self-absorption features, one of which had a blue profile. We have used the HCN (3–2) line, which may be more opaque in denser regions ($n_c = 6.8 \times 10^7$ cm^{-3} at $T_K = 100$ K) than CS (2–1).

2. OBSERVATIONS

The sample is a subset of a larger sample of dense cores associated with H_2O masers that have been surveyed with several CS transitions (Plume, Jaffe, & Evans 1992; Plume et al. 1997) and mapped in CS and dust emission (Shirley et al. 2003; Mueller et al. 2002). The sources mapped in CS (5–4) (Shirley et al. 2003) have virial masses within the nominal core radius (R_{CS}) ranging from 30 to 2750 $M_\odot$, with a mean of 920 $M_\odot$. That sample was selected to have CS (7–6) emission with $T_R^* \geq 1$ K. The sample for HCN observations was selected randomly from the sample in Shirley et al. (2003); we were trying to cover all the range of mass in that sample. This sample has a mean virial mass of 800 $M_\odot$. We used HCN (3–2) lines as the optically thick lines. The $H^{13}CN$ (3–2) lines or the $C^{34}S$ (5–4), (3–2), and (2–1) lines were used as optically thin lines. For comparison, CS (5–4) lines were also taken from our previous observations (Shirley et al. 2003).

All observations except the $C^{34}S$ (2–1) and (3–2) lines were made at the 10.4 m telescope at the Caltech Submillimeter

TABLE 1
OBSERVING PARAMETERS

Line	Date (UT)	ν[a] (GHz)	θ_{mb} (arcsec)	η_{mb}	v_{res} (km s^{-1})
HCN (3–2)	2002 Jun	265.886434	28.1	0.64	0.11
	2002 Dec	265.886434	28.1	0.60	0.11
$H^{13}CN$ (3–2)	2002 Dec	259.011814	28.9	0.60	0.11
	2003 May	259.011814	28.9	0.58	0.17
$C^{34}S$ (5–4)	2001 Jul	241.016089	31.0	0.73	0.12
$C^{34}S$ (2–1)	1991 Apr, Oct	96.4129495	25.0	0.60	0.31
$C^{34}S$ (3–2)	1990 Jun	144.617101	17.0	0.60	0.21
CS (5–4)	1997 Apr	244.935557	24.5	0.56	0.12

[a] The rest frequencies of HCN (3–2) and $H^{13}CN$ (3–2) have been updated according to Ahrens et al. 2002, and those of CS and $C^{34}S$ have been updated according to Gottlieb et al. 2003.

Observatory (CSO).[1] The $C^{34}S$ (2–1) and (3–2) data were taken from observations (Plume et al. 1997) at the IRAM 30 m telescope at Pico Veleta, Spain. The observing date, line frequency, beam size, main-beam efficiency, and velocity resolution of each line are listed in Table 1. The rest frequencies of the HCN (3–2), $H^{13}CN$ (3–2), and $C^{34}S$ lines have been updated (Ahrens et al. 2002; Gottlieb, Myers, & Thaddeus 2003) after our observations. We have corrected our data to the new frequencies listed in Table 1. The position-switching mode was used; offset positions were checked for HCN emission and found to be clear ($T_A^* < 0.5$ K). Pointing was checked periodically using planets and CO-bright stars. The pointing accuracy was better than 6″.

[1] The CSO is operated by the California Institute of Technology under funding from the National Science Foundation, contract AST 90-15755.

3. RESULTS

Table 2 lists our sources with their observed and derived parameters. Self-absorption features appeared in many sources. We characterize the line profiles by the velocity at the peak of the HCN (3–2) line, v_{thick}, by the velocity at the peak of the optically thin tracer, v_{thin}, and by the line width of the thin tracer, Δv_{thin}. Values were measured with a cursor or from a Gaussian fit, as appropriate. Moving clockwise from the lower left, Figure 1 illustrates the sample's range from a clearly blue profile (Fig. 1*a*) to a red profile (Fig. 1*d*).

A blue profile is a rather general feature of inflowing motion, but it only arises for the right combination of critical density and opacity of the line. It is predicted for velocity fields that decrease with radius, as in inside-out collapse models (Zhou & Evans 1994), but also for more general velocity fields (e.g., Myers et al. 1996). In a simple model with two uniform layers approaching each other (Myers et al. 1996), the shape of the profile is affected by both the optical depth of the line and the inflow velocity of the front layer (Myers et al. 2000). In the most opaque sources, as shown in Figure 1*a*, both the HCN (3–2) line and the CS (5–4) line show a blue profile, but the

TABLE 2
OBSERVED AND DERIVED PARAMETERS[a]

Source	R.A. (1950.0)	Decl. (1950.0)	Distribution (kpc)	v_{thick}[b] (km s^{-1})	v_{thin}[c] (km s^{-1})	Δv_{thin}[d] (km s^{-1})	δv	Profile[e]	log N[f] (CS)	$T_R^*(B)/T_R^*(R)$
RCW 142	17 47 04.5	−28 53 42	2.0	14.27(05)	17.24(05)[2]	5.60(12)	−0.53(02)	B	15.2	4.18(69)
W28 A2(1)	17 57 26.8	−24 03 54	2.6	10.55(05)	9.17(08)[1]	6.68(21)	0.21(01)	N	15.7	…
M8 E	18 01 49.1	−24 26 57	1.8	12.26(05)	10.65(10)[1]	3.34(27)	0.48(05)	R	14.8	0.95(08)
9.62+0.10	18 03 16.0	−20 32 01	7.0	7.11(06)	5.29(09)[1]	5.89(26)	0.31(02)	R	14.9	0.26(04)
10.60−0.40	18 07 30.7	−19 56 28	6.5	−6.51(05)	−4.51(08)[1]	6.93(18)	−0.29(01)	B	15.6	2.28(13)
19.61−0.23	18 24 50.1	−11 58 22	4.0	40.52(05)	42.16(15)[3]	7.18(29)	−0.23(02)	N	14.5	1.61(42)
23.95+0.16	18 31 40.8	−07 57 17	5.8	78.75(17)	80.15(09)[2]	2.39(22)	−0.59(11)	B	…	1.17(25)
W43 S	18 43 26.7	−02 42 40	8.5	96.83(05)	98.17(08)[1]	6.00(23)	−0.22(02)	N	14.0	1.68(15)
W44	18 50 46.1	+01 11 11	3.7	54.46(05)	57.20(08)[1]	5.78(10)	−0.47(01)	B	14.3	3.31(31)
35.58−0.03	18 53 51.4	+02 16 29	10.2	53.79(06)	54.04(15)[3]	5.16(27)	−0.05(03)	N	14.3	…
48.61+0.02	19 18 13.1	+13 49 44	11.8	17.87(05)	18.03(11)[2]	2.34(21)	−0.07(05)	N	14.1	…
59.78+0.06	19 41 04.2	+23 36 42	2.2	21.89(05)	22.63(07)[2]	2.21(23)	−0.33(05)	B	14.1	…
S88B	19 44 42.0	+25 05 30	2.1	22.30(11)	21.42(05)[2]	2.36(13)	0.37(05)	R	13.8	…
ON 2 S	20 19 48.9	+37 15 52	5.5	−0.05(05)	−0.90(06)[2]	3.65(14)	0.23(02)	N	14.3*	…
W75 N	20 36 50.5	+42 27 01	3.0	11.70(10)	9.26(08)[1]	5.47(07)	0.45(02)	R	14.4*	0.71(04)
DR 21 S	20 37 13.8	+42 08 52	3.0	−5.68(05)	−2.18(10)[4]	4.38(13)	−0.80(03)	B	14.4*	1.99(11)
W75(OH)	20 37 14.0	+42 12 12	3.0	−6.01(05)	−3.32(08)[1]	5.95(17)	−0.45(04)	B	14.8*	1.29(06)
Cep A	22 54 19.2	+61 45 44	0.7	−12.42(13)	−10.39(09)[2]	3.68(19)	−0.55(05)	B	14.5	1.06(07)
S158	23 11 36.1	+61 10 30	2.8	−59.46(11)	−56.23(12)[1]	6.15(29)	−0.53(03)	B	14.6*	1.78(20)
S157	23 13 53.1	+59 45 18	2.5	−45.05(11)	−43.82(10)[4]	2.56(20)	−0.48(07)	B	13.9*	1.39(33)
121.30+0.66	00 33 53.3	+63 12 32	1.2	−18.55(05)	−17.77(09)[1]	3.09(23)	−0.25(04)	N	14.0*	1.33(14)
123.07−6.31	00 49 29.2	+56 17 36	2.2	−32.67(05)	−30.84(11)[1]	4.68(28)	−0.39(04)	B	14.0*	1.27(28)
W3(OH)	02 23 17.3	+61 38 58	2.4	−49.39(05)	−46.85(08)[1]	5.18(20)	−0.49(03)	B	15.0*	1.44(15)
136.38+2.27	02 46 11.7	+61 47 34	4.5	−42.18(18)	−42.35(10)[4]	2.03(16)	0.08(10)	N	13.6*	…
S231	05 35 51.3	+35 44 16	2.3	−14.22(05)	−16.41(05)[1]	3.72(14)	0.59(03)	R	14.3	0.34(07)
S235	05 37 31.8	+35 40 18	1.6	−17.26(05)	−17.44(04)[1]	2.73(10)	0.07(02)	N	14.3*	…
S252A	06 05 36.5	+20 39 34	1.5	9.90(05)	9.10(06)[1]	2.57(14)	0.31(04)	R	…	…
S255/7	06 09 58.2	+18 00 17	1.3	6.80(10)	6.98(10)[4]	2.57(10)	−0.07(06)	N	14.3*	…

[a] Units of right ascension are hours, minutes, and seconds, and units of declination are degrees, arcminutes, and arcseconds. Distances are taken from Shirley et al. 2003 and Mueller et al. 2002. Quantities in parentheses give the uncertainties in units of 0.01.

[b] The velocity of the peak of the optically thick line, in this case HCN (3–2).

[c] The velocity of the peak of the optically thin line, whether $H^{13}CN$ (3–2) or $C^{34}S$ (5–4), (2–1), and (3–2), indicated by 1, 2, 3, and 4 respectively.

[d] FWHM of the optically thin line. For three sources [W28 A2(1), 9.62+0.10, and W44], we had to mask a strong wing component to get an accurate line width measurement.

[e] Profile of the line judged from δv. B denotes blue profile, R denotes red profile, and N denotes neither blue nor red.

[f] Taken from Plume et al. 1997, N is the column density derived from a large velocity gradient model fitted to several CS transitions. Densities with an asterisk are calculated from fitting several $C^{34}S$ transitions, corrected by the average difference of the log of the column densities, $\langle \log N(\mathrm{CS}) - \log N(\mathrm{C^{34}S}) \rangle = 0.83 \pm 0.27$.

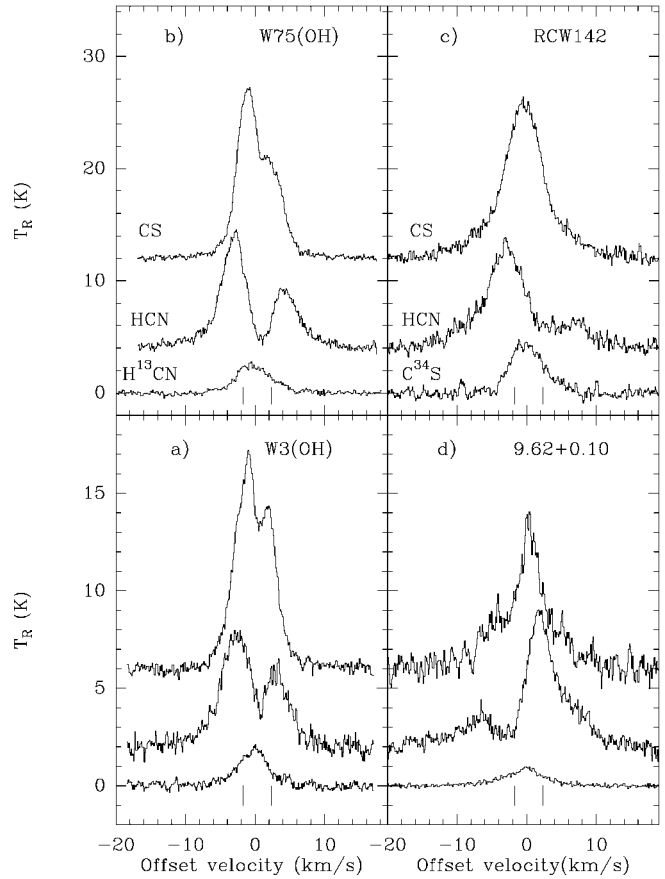

FIG. 1.—Line profiles of HCN (3–2) (*middle lines*), CS (5–4) (*upper lines*), and optically thin lines [*lower lines*; $H^{13}CN$ (3–2) for (*a*), (*b*), and (*d*) and $C^{34}S$ (5–4) for (*c*)]. HCN (3–2) and CS (5–4) lines have been displaced upward for clarity. All lines are plotted with the velocity relative to the optically thin line's central velocity. The two vertical lines below the spectra indicate the location of the outermost hyperfine components of the HCN (3–2) line. The radiation temperature T_R has been corrected for main-beam efficiency.

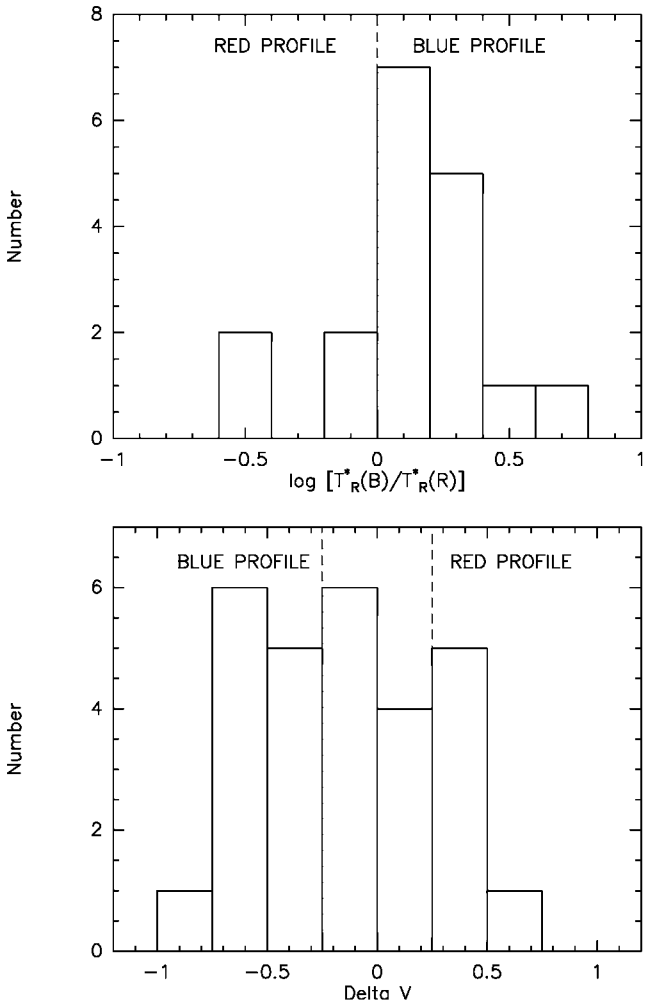

FIG. 2.—Distribution of log $[T_R^*(B)/T_R^*(R)]$ for the 18 double-peaked sources (*top plot*) and distribution of δv for all the 28 sources in the sample (*bottom plot*). Note that only 11 of the 14 blue sources and three of the four red sources in the top plot have ratios greater or less than unity by more than 1 σ.

HCN (3–2) line presents deeper absorption. As opacity drops, only HCN shows an absorption dip, as seen in Figure 1*b*, and the less opaque CS (5–4) line becomes a single peak with a red shoulder. If the inflow velocity is high enough, the red peak disappears, leaving only a flat wing as seen in Figure 1*c*.

The ratio of the blue peak to the red peak $[T_R^*(B)/T_R^*(R)]$ is one measure of the line asymmetry. A "blue profile" should have a stronger blue peak than red peak: $T_R^*(B)/T_R^*(R) > 1$ by a statistically significant amount. We calculated these ratios for the 18 sources with double-peaked spectra, as listed in Table 2. Eleven sources have a ratio of blue to red significantly greater than unity, and three have a ratio significantly less than unity; the other four cases do not differ from unity by more than 1 σ. The overall trend is a sign of the blue predominance in the sample.

Not all line profiles from collapsing cores will show two peaks; some will appear as lines skewed to the blue or lines with red shoulders. An alternative definition (Mardones et al. 1997) is useful for these cases as well. A line can be identified as a blue profile if the peak of the optically thick line is shifted blueward, with the velocity difference between the peaks of the optically thick line and the optically thin line greater than a quarter of the line width of the optically thin line: $\delta v = (v_{\rm thick} - v_{\rm thin})/\Delta v_{\rm thin} < -0.25$. A red profile would have $\delta v > 0.25$. The calculated δv for our sample are listed in Table 2. Twelve blue profiles and six red profiles were identified by this method, with statistically significant (≥ 1 σ) values of δv. The distributions of $T_R^*(B)/T_R^*(R)$ and δv are presented in Figure 2, which clearly shows the blue profile predominance.

The concept of the "excess" was introduced by Mardones et al. (1997) to quantify the statistics of the line asymmetry in a survey: $E = (N_{\rm blue} - N_{\rm red})/N_{\rm total}$, where $N_{\rm blue}$ and $N_{\rm red}$ are the numbers of blue and red profiles in the total sample of $N_{\rm total}$ sources (28 in the present case). Using the line ratios or the δv measure, the excesses in our sample are $E = 0.29$ and 0.21, respectively. For comparison, surveys of low-mass star-forming regions with HCO^+ (3–2) found $E = 0.30$, 0.31, and 0.31 for Class -1, Class 0, and Class I samples, respectively (Evans 2003). Although a single line with a blue profile may be explained by outflow or rotation, a large sample with a random distribution of angles between the outflow or rotation axis and the line of sight should result in a zero excess. A significant excess in a sample is statistical evidence of inflow. The probability that the observed number of blue and red sources could result from random sampling of a distribution that actually has equal numbers in blue and red bins, with the total equal to the actual total, is 0.03 for the intensity criterion and 0.16 for the δv criterion. The statistical significance is similar to that found for studies of low-mass regions by Gregersen et al. (2000).

4. DISCUSSION

Before accepting the inflow interpretation, we should examine other possible explanations for the line profiles. One possibility is that another molecular line contributes to the blue peak. The mean shift of the peak for the 12 blue profiles is $\langle v_{\rm thick} - v_{\rm thin} \rangle = -2.18 \pm 0.86$ km s^{-1}. Examination of transition catalogs revealed only two lines within ± 5 km s^{-1} of the HCN line that have energies above ground corresponding to less than 300 K: a line of glycolaldehyde shifted by -0.4 km s^{-1}, and a line of c-SiC_3 shifted by $+1.45$ km s^{-1}. Neither of these is likely to contribute significantly to the observed line profile. Accurate information on the hyperfine structure of the HCN (3–2) transition has been reported recently (Ahrens et al. 2002). The stronger components are all within 0.3 km s^{-1} of the line center; the two outer hyperfine components ($F = 2$–2 and 3–3) lie at -2.35 and 1.75 km s^{-1}, respectively. These outer components could affect the line profiles, but they have the same intrinsic line strengths, at 0.037 of the total line strength. Ahrens et al. (2002) found the blueshifted component ($F = 2$–2) to be anomalously *weak* in their observations of TMC-1. Thus, it seems unlikely that this component is contributing strongly to the blue peak, but it remains a remote possibility.

For 13 sources for which $H^{13}CN$ is not available, we used $C^{34}S$ as the optically thin line. Based on the nine sources for which we have both $H^{13}CN$ (3–2) and $C^{34}S$ (5–4) lines, the center velocity of $H^{13}CN$ (3–2) has a mean shift of -0.30 km s^{-1} relative to the center of the $C^{34}S$ (5–4) line, but the line width of the $H^{13}CN$ line is 1.24 times that of the $C^{34}S$ line. These facts suggest that $H^{13}CN$ (3–2) is not optically thin, and using it might make it harder to detect blue profiles. Indeed, using the $C^{34}S$ lines instead added two blue sources to the δv statistic, yielding an excess of 0.29, identical to that for the line ratio method. We conclude that the choice of optically thin line does not have a major effect on our statistics, but we have made a conservative choice by using $H^{13}CN$ lines where possible.

The self-absorption feature appears as long as the column density is high enough [log N(CS) $\geq$ 14.3 for this sample]. While HCN (3–2) works well for such dense, opaque cores, a different tracer may be needed for regions of lower column density. The two-layer model predicts that $|\delta v|$ should increase with optical depth (see Fig. 2 of Myers et al. 1996). We observe that $|\delta v|$ increases with log N(CS), although the correlation is weak. The relation between $|\delta v|$ and column density supports the idea that the blue profile only appears when the line has a suitable optical depth and critical density. The excesses based on the δv test for the CS (5–4) and (2–1) lines in this sample are $E = -0.04$ and 0.05, respectively. These negligible excesses are expected if the CS lines are less opaque in the inflow region.

The current work is only a promising indication that inflow in regions forming massive stars may be studied using HCN (3–2) lines. The sources in this sample span a wide range of distances; even if inflow motions are present, they may be related to the formation of individual stars in nearby regions and the formation of a cluster in more distant regions. In future work, we will extend the sample to sources with smaller column density. Maps will be made to test whether the blue profile peaks toward the center or whether it is associated with outflows. Sources that pass that test will become collapse candidates. Using the models of density and temperature established by observations of dust emission on the same sources (Mueller et al. 2002), we could then test some models of collapse to learn whether we are finally seeing gravitational infall in massive cores.

We are grateful to the staff of the CSO and to K. Allers, C. Knez, and Y. Shirley for assistance with the observations. We also thank Y. Shirley for use of his CS data before its publication. We thank G. Fuller and P. Myers for helpful comments on an earlier draft, and we thank the referee, M. Tafalla, for helpful comments and for alerting us to the updated frequencies for $C^{34}S$. This work was supported by NSF grant AST 99-88230 to the University of Texas at Austin and by the state of Texas.

REFERENCES

Ahrens, V., Lewen, F., Takano, S., Winnewisser, G., Urban, S., Negirev, A. A., & Koroliev, A. N. 2002, Z. Naturforsch., 57a, 669
Choi, M., Evans, N. J., II, Gregersen, E. M., & Wang, Y. 1995, ApJ, 448, 742
Dickel, H. R., & Auer, L. H. 1994, ApJ, 437, 222
Evans, N. J., II. 1991, in ASP Conf. Ser. 20, Frontiers of Stellar Evolution: 50th Anniversary McDonald Obs., ed. D. L. Lambert (San Francisco: ASP), 45
———. 2003, in Chemistry as a Diagnostic of Star Formation, University of Waterloo, Canada, 2002 August 21–23, ed. C. L. Curry & M. Fich, in press
Gottlieb, C. A., Myers, P. C., & Thaddeus, P. 2003, ApJ, 588, 655
Gregersen, E. M., & Evans, N. J., II. 2000, ApJ, 538, 260
Gregersen, E. M., Evans, N. J., II, Mardones, D., & Myers, P. C. 2000, ApJ, 533, 440
Gregersen, E. M., Evans, N. J., II, Zhou, S., & Choi, M. 1997, ApJ, 484, 256
Keto, E. R., Ho, P. T. P., & Haschick, A. D. 1988, ApJ, 324, 920
Lee, C. W., Myers, P. C., & Tafalla, M. 1999, ApJ, 526, 788
———. 2001, ApJS, 136, 703
Mardones, D., Myers, P. C., Tafalla, M., Wilner, D. J., Bachiller, R., & Garay, G. 1997, ApJ, 489, 719
Mueller, K. E., Shirley, Y. L., Evans, N. J., II, & Jacobson, H. R. 2002, ApJS, 143, 469
Myers, P. C., Evans, N. J., II, & Ohashi, N. 2000, in Protostars and Planets IV, ed. V. Mannings, A. P. Boss, & S. S. Russell (Tucson: Univ. Arizona Press), 217
Myers, P. C., Mardones, D., Tafalla, M., Williams, J. P., & Wilner, D. J. 1996, ApJ, 465, L133
Plume, R., Jaffe, D. T., & Evans, N. J., II. 1992, ApJS, 78, 505
Plume, R., Jaffe, D. T., Evans, N. J., II, Martin-Pintado, J., & Gomez-Gonzalez, J. 1997, ApJ, 476, 730
Shirley, Y. L., Evans, N. J., II, Mueller, K. E., Knez, C., & Jaffe, D. T. 2003, ApJ, submitted
Shu, F. H. 1977, ApJ, 214, 488
Welch, W. J., Dreher, J. W., Jackson, J. M., Terebey, S., & Vogel, S. N. 1988, Science, 238, 1550
Williams, J. P., & Myers, P. C. 1999, ApJ, 511, 208
Wolf-Chase, G. A., & Gregersen, E. 1997, ApJ, 479, L67
Zhang, Q., & Ho, P. T. P. 1997, ApJ, 488, 241
Zhang, Q., Ho, P. T. P., & Ohashi, N. 1998, ApJ, 494, 636
Zhou, S., & Evans, N. J., II. 1994, in ASP Conf. Ser. 65, Clouds, Cores, and Low Mass Stars: The Fourth Haystack Obs. Conf., ed. D. P. Clemens & R. Barvainis (San Francisco: ASP), 183
Zhou, S., Evans, N. J., II, Koempe, C., & Walmsley, C. M. 1993, ApJ, 404, 232
———. 1994, ApJ, 421, 854